Journal of Power Sources 269 (2014) 152–157

Contents lists available at ScienceDirect

Journal of Power Sources

journal homepage: www.elsevier.com/locate/jpowsour

Shape-dependent catalytic activity of oxygen reduction reaction (ORR) on silver nanodecahedra and nanocubes

Qiyu Wang [a], Xiaoqiang CUI [a, *], Weiming Guan [b], Lei Zhang [a], Xiaofeng Fan [a], Zhan Shi [c], Weitao Zheng [a, *]

[a] Department of Materials Science, Key Laboratory of Automobile Materials of MOE and State Key Laboratory of Superhard Materials, Jilin University, Changchun 130012 People's Republic of China
[b] State Key Laboratory of Advanced Technologies for Comprehensive Utilization of Platinum Metals, Kunming 650106, People's Republic of China
[c] State Key Laboratory of Inorganic Synthesis and Preparative Chemistry, College of Chemistry, Jilin University, Changchun 130012, People's Republic of China

HIGHLIGHTS

- Shape effects on ORR were studied on Ag nanostructures with different facets.
- The electrocatalytic activity is different on Ag nanodecahedra and nanocubes.
- The adsorption competition between oxygen and hydroxyl is crucial for ORR on Ag.
- The surface facet of Ag nanocrystals is important parameter to designing catalysts.

GRAPHICAL ABSTRACT

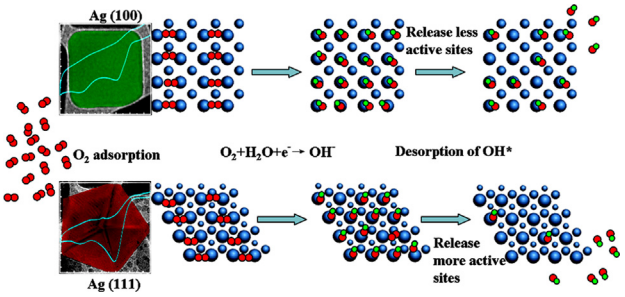

ARTICLE INFO

Article history:
Received 11 April 2014
Received in revised form
9 June 2014
Accepted 30 June 2014
Available online 7 July 2014

Keywords:
Silver
Nanodecahedra
Nanocubes
Oxygen reduction reaction
Electrocatalysis

ABSTRACT

The structure effects on the oxygen reduction reaction (ORR) are studied on similar sized silver nanodecahedra and nanocubes which are enclosed by (111) and (100) facets, respectively. The results show that the oxygen reduction proceeds one-step "direct" four-electron reduction on silver nanodecahedra, while two-step processes on silver nanocubes. The simulations results suggest that the different ORR catalytic activity can be interpretated by the adsorption competition between oxygen and hydroxyl on different silver facets. We demonstrate that the surface facet of silver nanocrystals is a decisive parameter to designing catalysts for ORR and other electrocatalytic reaction.

1. Introduction

Silver nanoparticles with unique properties [1] attract great attention of chemists in a wide variety of fields, such as optics [2,3], sensing [4–7], biological therapy [8] and catalysis [9,10]. Although metallic silver is usually considered to be catalytically sluggish for most reactions due to their filled *d* bands, it has been proved that silver nanostructures can act as an active catalyst for the oxidation of olefins [11] or ethylene epoxidation [9,10]. The size, shape, and morphology of silver nanostructures all play significant roles on the electrocatalytic oxidation reactions [12–15]. Recently, nanosized silver catalyst shows a promising potential to be an alternative to

* Corresponding authors. Tel./fax: +86 431 85155279.
E-mail addresses: xqcui@jlu.edu.cn (X. CUI), wtzheng@jlu.edu.cn (W. Zheng).

http://dx.doi.org/10.1016/j.jpowsour.2014.06.160
0378-7753/

platinum for oxygen reduction reaction (ORR) under alkaline condition [16,17] to lower down the high-cost of platinum-based cathodic catalyst in electrochemical fuel cell [18–21]. Chen's group has shown that the size and protective agent perform big effects on the electrocatalytic ORR behavior of silver nanostructures [16,22]. However, the shape and structure effect of silver nanostructures for ORR still remains unclear up to now.

In this study, we chose two kinds of silver nanostructures, namely nanodecahedra and nanocubes, for investigating the shape effect on ORR. Nanodecahedra are surrounded by ten Ag (111) facets, while nanocubes are surrounded by six Ag (100) facets. The structure and morphology of nanostructures are characterized with UV–vis absorption spectroscopy, X-ray diffraction (XRD) and transmission electron microscope (TEM). Their electrocatalytic performances in alkaline solution are investigated by cyclic and rotating disk voltammetry. We found that the oxygen reduction on nanodecahedra precedes the most efficient four-electron reduction, but that on nanocubes precedes a two-step pathway. That means nanodecahedra have higher activity than nanocubes for ORR in alkaline solution. The electrocatalytic difference is explained by simulation results on the adsorption energy of oxygen and hydroxyl on silver (111) and (100) facets. This finding will give a deep insight for designing silver nanostructures as an effective catalyst in alkaline based fuel cells.

2. Experimental

2.1. Materials

Silver nitrate ($AgNO_3$, 99.8%) was purchased from Adamas-beta Chemical Co (Switzerland). Trisodium citrate (99.0%) was obtained from Beijing Chemical Plant (Beijing, China). $NaBH_4$ (96.0%), ethylene glycol and poly(vinyl pyrrolidone) (PVP, M.W.≈30,000) were obtained from Sinopharm Chemical Reagent Co., Ltd (China). Sodium hydrosulfide was purchased from Xiya Chemical Reagent Company (China). All chemicals were used without further purification.

2.2. Instruments

LED lamp was obtained from Shanghai Yaming Lighting Co., Ltd. Transmission electron-microscopy (TEM) images were taken with a Tecnai F20 transmission electron microscope (FEI Co., Japan). Silver nanoparticles were characterized by UV–vis spectroscopy (CHEMUSB4000-UV/vis, Ocean Optics Inc.) and X-ray diffraction (XRD) diffractometer (Bragg-Brentano diffractometer, D8-tools, a Cu-Kα line at 0.15418 nm). Electrochemical measurements were carried out on a CHI650D workstation from Chenhua Co., (Shanghai, China). A three-electrode cell was used with the modified glassy carbon electrode (GCE) as the working electrode, an Ag/AgCl (in saturated KCl) as the reference electrode and a platinum foil electrode as the counter electrode.

2.3. Sample preparation

2.3.1. Preparation of silver nanodecahedra

Silver nanodecahedra were synthesized according to previous reported photomediated method [6]. For preparation of silver seeds, ultrapure water (88 mL), $AgNO_3$ (1 mL, 10 mM), and sodium citrate (10 mL, 10 mM) were added into a 250 mL flask that immersed in ice bath and stirred for 30 min. Aqueous $NaBH_4$ (0.8 mL, 10 mM) was added drop-wise into the solution with a rate of 0.2 mL min^{-1}. The colorless solution turned to bright yellow after 2 min. The bright yellow solution was then immediately exposed to the LED lamp (460 nm) for 5 h at 30 °C. The final products were washed with ethanol and water for three times each by centrifugation.

2.3.2. Preparation of silver nanocubes

The synthetic of silver nanocubes is similar to the literature of Xia's group with small modification [23]. In a typical synthesis, 60 mL of ethylene glycol (EG) was added into a round-bottom flask in an oil bath. EG solution was kept at 150 °C for 50 min under magnetic stirring with a flow of N_2 via a glass pipette. 0.7 mL of a NaHS solution in EG (3 mM) and 15 mL of PVP solution in EG (0.18 mM) were quickly injected into the reaction system. After 8 min, 5 mL of $AgNO_3$ (0.28 M) solution in EG was added into the flask. The reaction solution was heated for about 20 min after the addition of $AgNO_3$, and then quenched by placing the reaction solution in acetone. In order to remove most of EG and PVP, the samples were subsequently washed with acetone, ethanol, and water for 5 times by centrifugation.

2.4. Preparation of silver nanostructure-modified electrodes

Glassy carbon electrodes (GCE, 3 mm in diameter, CHI Instruments) are sequentially polished with Al_2O_3 (1, 0.3 and 0.05 μm) slurry, and then dried at room temperature. The ink of silver nanostructures is prepared by dispersion of nanodecahedra or nanocubes in ultrapure water with ultrasonic. 4 μL of the ink is then dropped on the GC electrodes and then dried in vacuum. The working electrodes are denoted as Ag–NDs/GCE (nanodecahedra) and Ag–NCs/GCE (nanocubes).

2.5. Computational method

The density functional theory (DFT) calculations were performed to explore the adsorption of O_2 and OH on silver nanocrystal surfaces. The method of projector- augmented wave potentials were employed as implemented in the Vienna ab initio simulation package (VASP) code [24,25]. The generalized gradient approximation (GGA) with the parametrization of Perdew–Burke–Ernzerhof (PBE) is used to express the exchange-correlation energy of interacting electrons [26]. The dipole correction was considered. The kinetic energy cutoff of 550 eV was used for the plane wave expansion. The Monkhorst-Pack method is used to sample the k points in the Brillouin zone. The (100) and (111) surfaces of silver were modeled with 2 × 2 slab with seven layers. In the models, the vacuum separation was set to 18 Å in order to avoid the spurious coupling effect. Only the one layer in the middle along the z direction was fixed to the bulk positions during the relaxation. The Brillouin zones are sampled with the Γ-centered k-point grid of 3 × 3 × 1.

3. Results and discussion

3.1. Characterization of silver nanostructures

Silver nanodecahedra and nanocubes were prepared according to the previous reports [7,23]. As-prepared nanostructures were first characterized by UV–vis absorption spectra, as shown in Fig. 1(A). Both silver nanostructures show similar shape with two peaks corresponding to the longitudinal and transverse modes of localized surface plasmon resonance (LSPR) bands [27,28]. The position of the dominant peak from longitudinal mode is usually used to estimate the size of silver nanostructures. Nanodecahedra show a major adsorption at 493 nm indicating that the edge is of about 35 nm from the previous reports [7,29]. The dominant peak at 440 nm of nanocubes indicates that the size is of about 37 nm [30,31]. The narrow peaks show that the products are with a

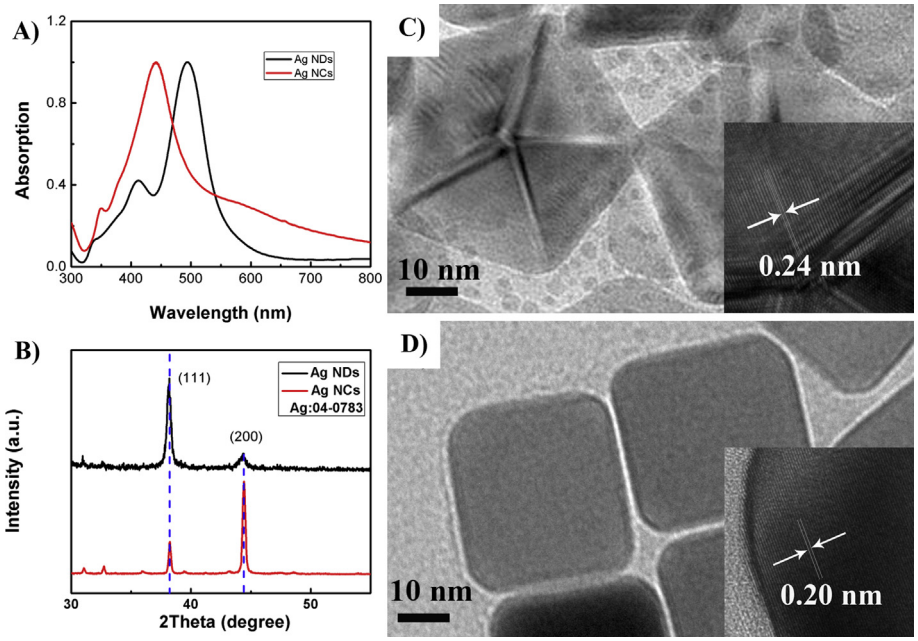

Fig. 1. (A) UV–vis spectra, and (B) XRD of silver nanodecahedra (black) and nanocubes (red). The silver from the JCPDS is shown as blue dash line. TEM images of silver (C) nanodecahedra and (D) nanocubes used in this study. The insets are the corresponding HRTEM of silver (C) nanodecahedra, and (D) nanocubes. (For interpretation of the references to color in this figure legend, the reader is referred to the web version of this article.)

symmetric shape and good size monodispersity. XRD was used to examine the crystalline phase of silver nanostructures, as shown in Fig. 1(B). Two diffraction peaks at 38.1° and 44.3° are indexed to the crystalline planes (111) and (200) of center faced cubic structures of silver in JCPDS (NO.04-0783). The significant differences of the ratio of peak intensity from (111) to (200) indicate that the main crystal facet of nanodecahedra is (111), while the nanocubes are surrounded by (100) facets [32]. The morphologies of silver nanostructures are further characterized by TEM, as shown in Fig. 1(C and D). Both silver nanostructures are very uniform. The average edge is of 35 ± 4 nm for nanodecahedra, and is of 37 ± 2 nm for nanocubes, which are in good agreement with the estimation from UV–vis results. HRTEM image in the inset of Fig. 1(C) shows that the interplanar spacing of the lattice fringes is of 0.24 nm for nanodecahedra, which is ascribed to the (111) plane of silver crystal [33]. For silver nanocubes, the interplanar spacing of the lattice fringes is of 0.20 nm, which is ascribed to the (100) plane of silver crystal, as shown in the inset of Fig. 1(D) [34]. The results of HRTEM images are in agreement with the XRD data.

3.2. Electrochemical characterization

3.2.1. Cyclic voltammetry of silver nanostructures

The electrochemical performance of the silver nanostructures is investigated with cyclic voltammetry. XPS (X-ray photoelectron spectroscopy) was used to identify the adsorption on Ag nanostructure layers, as shown in Fig. S1. The results indicated that the catalysts surfaces had been cleaned up with few of residual adsorbates. Fig. 2 shows the cyclic voltammetric behavior of silver nanodecahedra and nanocubes in 0.1 M KOH saturated with N_2. Three anodic peaks are observed at 0.20, 0.27 and 0.37 V during the positive scan on the silver nanodecahedra surface, as shown in Fig. 2(A). The first peak at 0.20 V is ascribed to the formation of a few monolayers of AgOH and Ag (I) species. The formation of bulk phases of AgOH and Ag_2O results in the other two peaks at 0.27 and 0.37 V, respectively. In the negative scan, the cathodic current peak at 0.05 V is attributed to the electroreduction of the silver oxide [16]. The reduction charge of the Ag oxides was employed to estimate electrochemical active area values for the Ag catalysts based on the charge density for the formation of Ag oxide monolayer (the detail calculation procedure was shown in Supporting

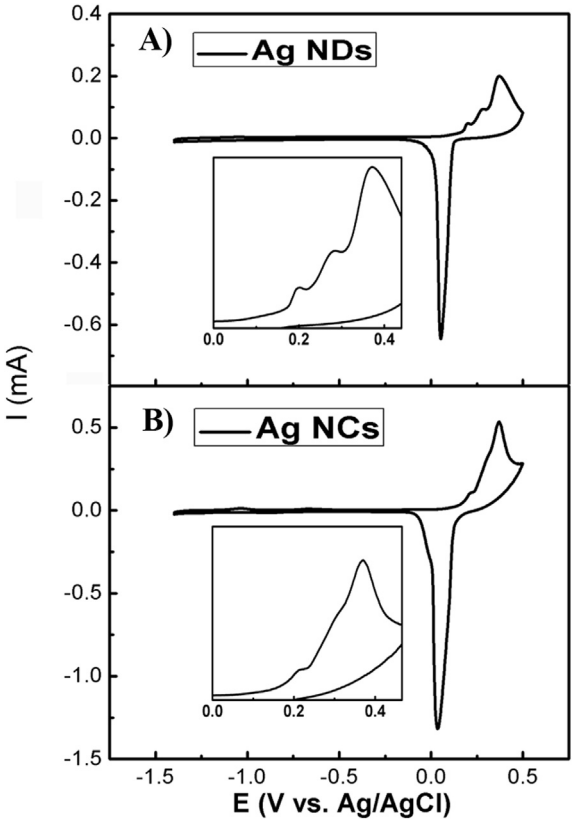

Fig. 2. CVs at GC modified with silver nanodecahedra (A) and nanocubes (B) at a sweep rate of 0.1 V s^{-1} in N_2-saturated 0.1 M KOH.

Information). For the silver nanocubes, three anodic peaks appear at the similar potential during the positive scan. However, the peak at 0.37 V is broader and stronger than that on silver nanodecahedra, which may be explained by the easier oxidation to form compact outer oxide layer on the surface of silver nanocubes because of the higher free energy of (100) facet [35]. The reduction potential of silver oxides on silver nanocubes negatively shifts to 0.04 V from 0.05 V obtained on silver nanodecahedra. It indicates that the silver oxide on silver nanodecahedra is easier to be reduced than that on silver nanocubes. This can be anticipated by the fact that the oxygen-contained species show more favorable adsorption energy on (100) than that on (111) facet of silver [36]. The different CV features from Ag-NDs/GC and Ag–NCs/GC imply that the electrocatalytic behavior of silver nanostructures should be shape-dependent.

Fig. 3 shows the cyclic voltammograms of Ag–NDs/GC and Ag–NCs/GC electrodes in 0.1 M KOH that was saturated with O_2 or N_2. The voltammetric currents have been normalized to the electrochemically active surface areas according to the oxygen adsorption measurement method proposed by Trasatti and Petrii [37]. Ag–NDs/GC shows no obvious electrochemical response in N_2-saturated KOH within the potential range of −1.2 to +0.1 V (Ag–NCs/GC shows similar results, data not shown). Two distinguished reduction current peaks appear at around −0.4 and −0.9 V on both electrodes when the electrolyte solution is saturated with O_2. We anticipate that the reduction current peaks shown in Fig. 3 come directly from the oxygen reduction based on the fact that there is no reduction current from silver oxides (blue curve) [16]. The peak current density and onset potentials are the most important two parameters in the quantitative assessments of the activity of the electrocatalysts [38]. Although two kinds of silver nanostructures have similar onset potential at approximately −0.08 V, their cathodic peak currents and shapes show significant difference in Fig 3. Take the case of silver nanodecahedra, the current density of reduction peak at −0.42 V (−2.31 mA cm^{-2}) is higher than that at −0.91 V (−1.68 mA cm^{-2}). For the silver nanocubes, the current density at −0.90 V (−1.93 mA cm^{-2}) is higher than −0.38 V (−1.49 mA cm^{-2}). Such voltammetric features clearly suggest that the silver nanodecahedra and nanocubes exhibit different electrocatalytic pathway for ORR [39].

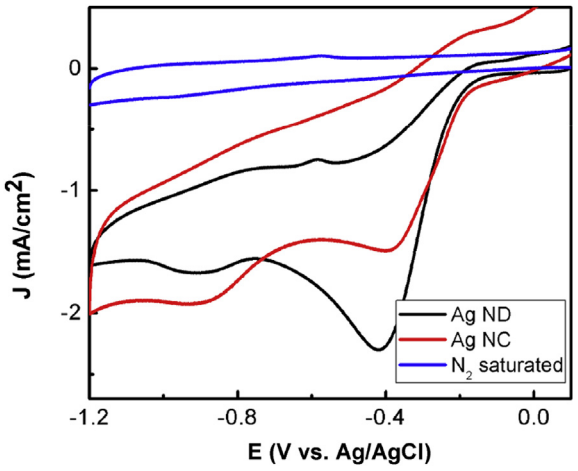

Fig. 3. CVs of Ag–NDs/GC in N_2-saturated (blue) and O_2-saturated (black) 0.1 M KOH and of Ag–NCs/GC in O_2-saturated (red) 0.1 M KOH. Potential scan rate: 0.1 V s^{-1}. (For interpretation of the references to color in this figure legend, the reader is referred to the web version of this article.)

3.2.2. Rotating disk voltammetry of silver nanostructures

To further reveal the electrocatalytic activity, the reaction kinetic of ORR at silver nanodecahedra and nanocubes were also studied with rotating disk voltammetry. Fig. 4 shows a series of rotating disk voltammograms (RDVs) of ORR recorded on the Ag–NDs/GC and Ag–NCs/GC at different rotation rates (from 225 to 3600 rpm) in an oxygen-saturated 0.1 M NaOH solution. For the RDVs on silver nanodecahedra shown in Fig. 4(A), only one stage of limiting current can be observed during the oxygen reduction process, suggesting the electrocatalytic reduction of oxygen proceeds is one-step processes. However, the RDVs of ORR on silver nanocubes in Fig. 4(B) show that two stages of limiting current can be obtained at about −0.6 V and −1.0 V, respectively, indicating electrocatalytic reduction of oxygen proceeds via two-step processes.

The Koutecky–Levich plots (shown in Fig 4(C and D)) are used to analyze the electron transfer numbers for ORR on silver nanostructures at different potentials based on the Koutecky–Levich equation:

$$\frac{1}{J}=\frac{1}{J_K}+\frac{1}{J_L}=\frac{1}{J_K}+\frac{1}{B\omega^{1/2}} \tag{1}$$

$$B=0.62nFC_oD_o^{2/3}\upsilon^{-1/6} \tag{2}$$

$$J_K=nFkC_o \tag{3}$$

in which J is the measured current density, J_K and J_L are the kinetic and diffusion limiting current densities, ω is the angular velocity of the disk ($\omega=2\pi N$, N is the rotation speed), n is the overall number of electrons transferred in oxygen reduction, F is the Faraday constant (F = 96485 C mol^{-1}), C_o is the bulk concentration of O_2 ($C_o=1.2\times10^{-3}$ mol L^{-1} in 0.1 M KOH solution), D_o is the diffusion coefficient for O_2 ($D_o=1.9\times10^{-5}$ cm^2 s^{-1} in 0.1 M KOH solution), υ is the kinematic viscosity of the electrolyte (υ = 0.01 cm^2 s^{-1} in 0.1 M KOH solution), and k is the electron transfer rate constant [40,41]. According to Equations (1) and (2), the electron transfer number (n) on silver nanodecahedra was calculated to be 3.8 ($\approx$4) at −0.60 to −1.0 V based on the slopes of Koutecky–Levich plots in Fig. 4(C). Fig. 4(D) depicts the Koutecky–Levich plots of silver nanocubes modified electrode at various potentials from −0.59 to −1.04 V. The numbers of electrons transferred are determined to be 3.1 at the first (−0.59 and −0.69 V) and 3.7 at the second (−0.88 and −1.04 V) stage.

The results of CVs and RDVs indicate that the ORR on silver nanodecahedra proceeds via the most efficient four-electron process:

$$O_2+2H_2O+4e^-\rightarrow4OH^- \tag{4}$$

Whereas the electrocatalytic reduction of oxygen on silver nanocubes proceeds via two-step processes:

$$O_2+H_2O+2e^-\rightarrow OH^-+HO_2^- \tag{5a}$$

$$HO_2^-+H_2O+2e^-\rightarrow3OH^- \tag{5b}$$

The electrocatalytic activity sequence is also in agreement with the experimental results on single-crystal bulk Ag electrodes in 0.1 M KOH [42].

3.3. Mechanisms of ORR on silver nanostructures

The silver nanostructures we investigated in this work were designed in similar dimension to eliminate the size effect of

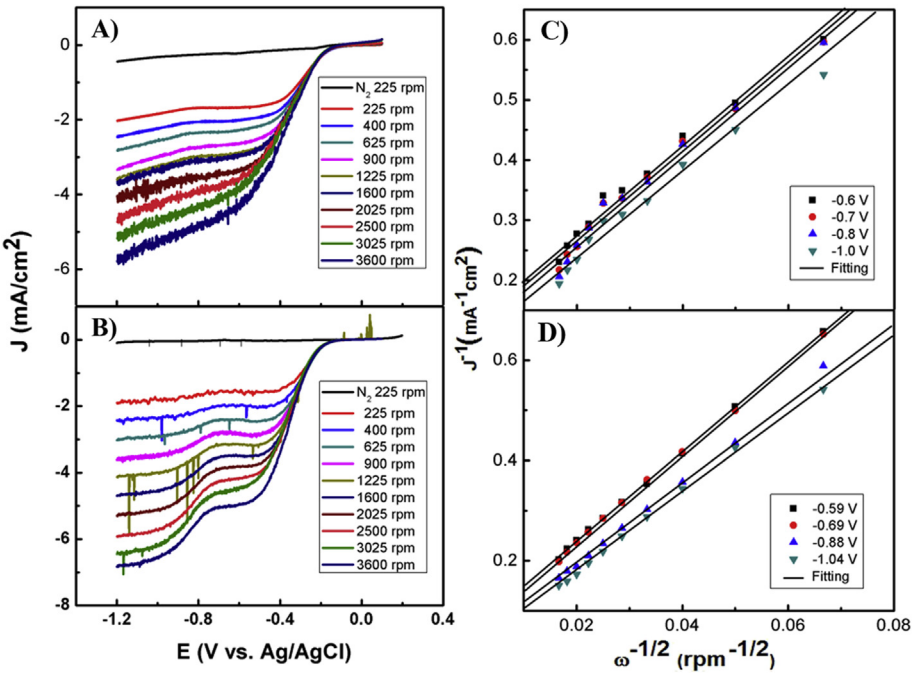

Fig. 4. Rotating disk voltammograms recorded on Ag–NDs/GC (A) and Ag–NCs/GC (B) in 0.1 M KOH saturated with oxygen at different rotation rates (shown as figure legends). Potential scan rate: 0.02 V s^{-1}. Koutecky–Levich plots (J^{-1} vs $\omega^{-1/2}$) for Ag–NDs/GC (C) and Ag–NCs/GC (D) at different potentials (shown as figure legends). Symbols are experimental data obtained from the corresponding rotating disk voltammograms shown in Fig. 4 (A, B). Lines are the linear regressions.

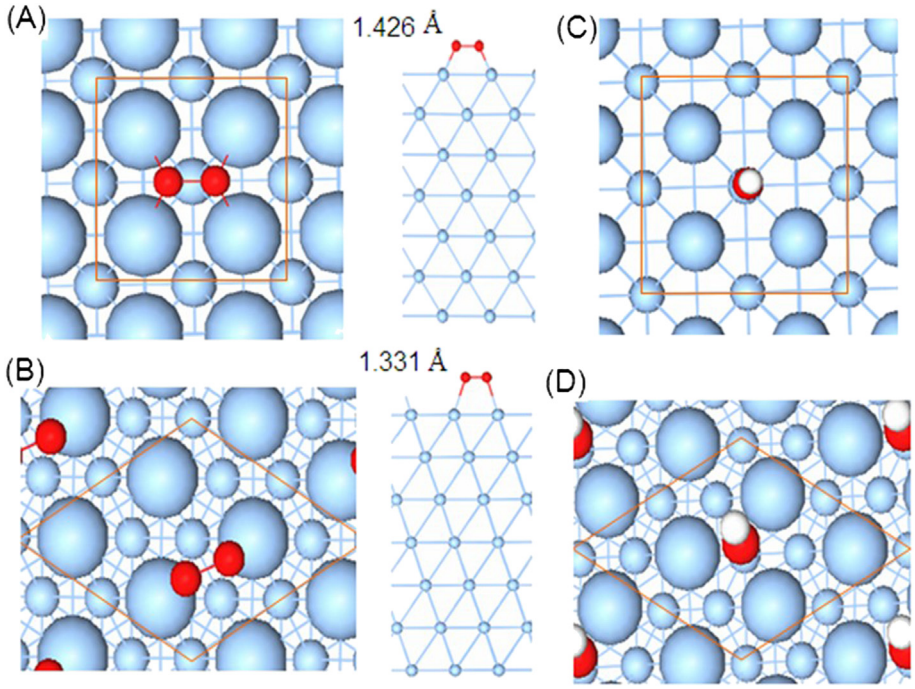

Fig. 5. The most favorable adsorption configurations of O_2 on silver (100) facet (A) and silver (111) facet (B) with top and side view and that of OH on silver (100) facet (C) and on silver (111) facet (D).

nanostructures [22,43]. The only difference should be taking into account is their structures, in which the silver nanodecahedra are mainly surrounded with (111) facets, and the silver nanocubes are surrounded with (100) facets [11,44]. The kinetics of ORR on silver nanostructures is controlled by the parameters of the energy of molecule O_2 adsorption, reaction intermediates, and the available active sites on surface that are affected mainly by the adsorption of hydroxyl in alkaline solution [45]. To simplify the system, we simulate the adsorption energy of oxygen and hydroxyl on silver (111) and (100) to explain the electrocatalytic activity difference.

Several configurations for the O_2 molecular adsorbed on both surfaces are considered and the most favorable configuration on Ag

(100) and that on Ag (111) on the basis of adsorption energy are shown in Fig. 5. For the adsorption of O_2 on the Ag (100), O_2 is settled on the hollow site confined by the under Ag atoms with an adsorption energy of 1.43 eV. The O_2 on the Ag (111) is adsorbed on the bridge site of two neighbor silver atoms with a adsorption energy of 0.85 eV. The both configurations are similar to that on Pt (100) and Pt (111) [46]. The charge transfer from the surface to O_2 is found for both surface and results in the elongation of O–O bond. The bond length (1.426 Å) of O_2 adsorbed on Ag (100) is slightly larger than that (1.331 Å) on Ag (111). In addition, the bond lengths of O_2 on both surfaces are larger than that of the isolated O_2 molecule (1.23 Å). This means the silver surfaces can activate the O_2 molecule and the adsorption on (100) surface is more effective than that on (111) surface. The higher adsorption energy of O_2 on Ag (100) surface means that the Ag (100) will have lower activation energy in the second process of ORR than the Ag (111), which is in contrast to the experimental results.

Following the applied potential, the hydroxyl is absorbed on the silver surface. The increase of the HO* on surface will limit the adsorption of O_2 and HOO*, since the active sites on the surface is decreased due to the coverage of HO*. The formation of OH* on both surfaces is simulated. It is found that the HO* likes to occupy the hollow sites for both surfaces as shown in Fig. 5(C and D). Based on the results of our simulation, the adsorption energy of OH* on Ag (100) surface is 0.23 eV larger than that on Ag (111). Therefore, the ratio of OH* coverage on Ag (100) is higher than that on Ag (111) due to the easy adsorption of OH* on Ag (100). The superfluous HO* formation on surface will block the formation of HOO* and be possible to lead to the desorption of $H_2O_{2,ad}$. Thus, the possibility of two-electrons pathway is increased for Ag (100) surface, though the O–O bond on Ag (100) is easier to be broken to yield the four-electron reduction. The balance of two factors results in the four-electron process on Ag (111) surface is more popular than that on Ag (100) surface as the observation in the experiment on silver nanodecahedra and silver nanocubes.

4. Conclusions

Uniform silver nanodecahedra and nanocubes with similar size are synthesized to investigate the shape effect on ORR. The electrochemical data proved that oxygen proceeds a “direct” four-electron reduction process on silver nanodecahedra surface, while a two-step process on silver nanocubes. We employed the simulation data to elucidate the different catalytic activity of ORR on silver nanostructure surfaces. It was demonstrated that the weaker adsorption of OH* on silver (111) facet provides more active sites, leading to the higher catalytic activity of ORR on silver nanodecahedra than that on silver nanocubes.

Acknowledgments

This work was financially supported by the National Natural Science Foundation of China (No. 21275064, 21075051), Program for New Century Excellent Talents in University (NCET-10-0433), Specialized Research Fund for the Doctoral Program of Higher Education (20130061110035), the fund of the State Key Laboratory of Advanced Technologies for Comprehensive Utilization of Platinum Metals (SKL-SPM-201207).

Appendix A. Supplementary data

Supplementary data related to this article can be found at http://dx.doi.org/10.1016/j.jpowsour.2014.06.160.

References

[1] B. Wiley, Y. Sun, Y. Xia, Acc. Chem. Res. 40 (2007) 1067.
[2] C.J. Murphy, T.K. Sau, A.M. Gole, C.J. Orendorff, J. Gao, L. Gou, S.E. Hunyadi, T. Li, J. Phys. Chem. B 109 (2005) 13857.
[3] Z. Xu, Y. Hou, S. Sun, J. Am. Chem. Soc. 129 (2007) 8698.
[4] A.J. Marenco, D.B. Pedersen, S. Wang, M.W. Petryk, H.B. Kraatz, Analyst 134 (2009) 2021.
[5] Y. Bonfil, M. Brand, E. Kirowa-Eisner, Electroanalysis 15 (2003) 1369.
[6] Y. Lu, G.L. Liu, L.P. Lee, Nano Lett. 5 (2005) 5.
[7] H. Wang, X. Zheng, J. Chen, D. Wang, Q. Wang, T. Xue, C. Liu, Z. Jin, X. Cui, W. Zheng, J. Phys. Chem. C 116 (2012) 24268.
[8] J.Z. Zhang, J. Phys. Chem. Lett. 1 (2010) 686.
[9] P. Christopher, S. Linic, J. Am. Chem. Soc. 130 (2008) 11264.
[10] P. Christopher, H. Xin, S. Linic, Nat. Chem. 3 (2011) 467.
[11] R. Xu, D. Wang, J. Zhang, Y. Li, Chem.-Asian J. 1 (2006) 888.
[12] V. Bansal, V. Li, A.P. O'Mullane, S.K. Bhargava, CrystEngComm 12 (2010) 4280.
[13] J. Geng, Y. Bi, G. Lu, Electrochem. Commun. 11 (2009) 1255.
[14] M. Chatenet, F. Micoud, I. Roche, E. Chainet, Electrochim. Acta 51 (2006) 5459.
[15] S. Linic, P. Christopher, H. Xin, A. Marimuthu, Acc. Chem. Res. 46 (2013) 1890.
[16] Y. Lu, Y. Wang, W. Chen, J. Power Sources 196 (2011) 3033.
[17] J. Guo, A. Hsu, D. Chu, R. Chen, J. Phys. Chem. C 114 (2010) 4324.
[18] B. Wang, J. Power Sources 152 (2005) 1.
[19] Q. Zhou, C.M. Li, J. Li, J. Lu, J. Phys. Chem. C 112 (2008) 18578.
[20] Y. Xiao, C.M. Li, Electroanalysis 20 (2008) 648.
[21] S. Guo, S. Zhang, L. Wu, S. Sun, Angew. Chem. 124 (2012) 11940.
[22] Y. Lu, W. Chen, J. Power Sources 197 (2012) 107.
[23] Q. Zhang, C. Cobley, L. Au, M. McKiernan, A. Schwartz, L.P. Wen, J. Chen, Y. Xia, ACS Appl. Mater. Interfaces 1 (2009) 2044.
[24] G. Kresse, J. Furthmüller, Phys. Rev. B 54 (1996) 11169.
[25] G. Kresse, D. Joubert, Phys. Rev. B 59 (1999) 1758.
[26] J.P. Perdew, J. Chevary, S. Vosko, K.A. Jackson, M.R. Pederson, D. Singh, C. Fiolhais, Phys. Rev. B 46 (1992) 6671.
[27] J. Zeng, Y. Zheng, M. Rycenga, J. Tao, Z.Y. Li, Q. Zhang, Y. Zhu, Y. Xia, J. Am. Chem. Soc. 132 (2010) 8552.
[28] C. Noguez, J. Phys. Chem. C 111 (2007) 3806.
[29] B. Pietrobon, V. Kitaev, Chem. Mater. 20 (2008) 5186.
[30] Q. Zhang, W. Li, L.P. Wen, J. Chen, Y. Xia, Chem.-Eur. J. 16 (2010) 10234.
[31] S.E. Skrabalak, L. Au, X. Li, Y. Xia, Nat. Protoc. 2 (2007) 2182.
[32] B. Wiley, Y. Sun, B. Mayers, Y. Xia, Chem.-Eur. J. 11 (2005) 454.
[33] S. Wang, H. Qian, Y. Hu, W. Dai, Y. Zhong, J. Chen, X. Hu, Dalton Trans. 42 (2013) 1122.
[34] T. You, S. Xu, S. Sun, X. Song, Mater. Lett. 63 (2009) 920.
[35] Y. Sun, Y. Xia, Science 298 (2002) 2176.
[36] P. Singh, D.A. Buttry, J. Phys. Chem. C 116 (2012) 10656.
[37] S. Trasatti, O. Petrii, J. Electroanal. Chem. 327 (1992) 353.
[38] W. Chen, S. Chen, Angew. Chem. Int. Ed. 48 (2009) 4386.
[39] S. Wang, D. Yu, L. Dai, J. Am. Chem. Soc. 133 (2011) 5182.
[40] C.L. Lee, H.P. Chiou, C.M. Syu, C.C. Wu, Electrochem. Commun. 12 (2010) 1609.
[41] L. Wu, H. Feng, M. Liu, K. Zhang, J. Li, Nanoscale 5 (2013) 10839.
[42] B. Blizanac, P. Ross, N. Markovic, J. Phys. Chem. B 110 (2006) 4735.
[43] W. Tang, H. Lin, A. Kleiman-Shwarsctein, G.D. Stucky, E.W. McFarland, J. Phys. Chem. C 112 (2008) 10515.
[44] S. Mostafa, F. Behafarid, J.R. Croy, L.K. Ono, L. Li, J.C. Yang, A.I. Frenkel, B.R. Cuenya, J. Am. Chem. Soc. 132 (2010) 15714.
[45] D.W. Boukhvalov, Y.W. Son, Nanoscale 4 (2012) 417.
[46] R. Long, K. Mao, X. Ye, W. Yan, Y. Huang, J. Wang, Y. Fu, X.S. Wang, X. Wu, Y. Xie, J. Am. Chem. Soc. 135 (2013) 3200.